Surface Review and Letters, Vol. 15, No. 5 (2008) 567–579

World Scientific
www.worldscientific.com

A DENSITY-FUNCTIONAL-THEORY STUDY OF MAGNETIC ANISOTROPIES OF ONE-DIMENSIONAL Ni CHAINS AND MAGNETISM OF 3D TRANSITION METALS ON Au(110)-(1 × 2) SURFACE

WEI FAN
Key Laboratory of Materials Physics,
Institute of Solid State Physics, Chinese Academy of Sciences,
230031-Hefei, People's Republic of China
fan@theory.issp.ac.cn

XIN-GAO GONG
Department of Physics, Fudan University,
200433-Shanghai, People's Republic of China

Received 6 January 2008

Based on the Density Functional Theory (DFT) with noncollinear-magnetism formulations, we have calculated the magnetism of single 3d transition-metal atoms and the magnetic anisotropies of supported Ni chains on the Au(110)-(1 × 2) surface. Our results for single absorbed 3d transition-metal atoms show that the surface relaxations enhance the orbital moments of left-end elements (Ti, V) and quenches the orbital moments of right-end elements (Fe, Co, Ni) on the Au(110)-(1 × 2) surface. The magnetic anisotropies of Ni atomic chains on the surface are closely related to orbital quenching. The easy magnetized axes change from the direction parallel to the chains to the direction perpendicular to the Ni chains when they absorb on the surface.

Keywords: Magnetic anisotropy; one-dimensional magnetism; surface reconstruction; noncollinear density functional theory.

1. Introduction

The high-density magnetic recording and the memory devices require strong magnetic anisotropy. The low-dimensional materials due to the reduced dimensionality generally have a favorable direction, and the physical properties along this direction are generally different from the other directions. Thus, we have the most possibilities to find the strong magnetic anisotropy materials from these low-dimensional materials. On the other hand, the reduced dimensionality reduces the atomic coordination number and enhances the spin and orbital magnetic moments of the materials. Since the pioneering experiments for the magnetism of Fe strips on the W(110) and Cu(111) surfaces,[1–4] the researches along this direction have been extended to other quasi-one-dimensional systems such as the monatomic magnetic chains on the vicinal surface,[5–7] and Co magnetic dot-chain on the Ru(0001) surface.[8] The transition from in-plane to out-of-plane magnetic anisotropy had been found in Fe nanostructure when it approaches the one-dimensional limit.[9] Besides the celebrating properties such as the strong magnetic anisotropy and the enhanced spin and orbital moments, some new phenomena have been found, such as the temperature and time-dependent magnetization[1,2] which make the realistic applications of these novel devices face new serious problems such as the instability of magnetic structures.

It is valuable to investigate theoretically the magnetic stability of surface-supported novel structures.[10] Many theoretical and computational methods have been used to study the magnetism of one-dimensional structures on surfaces such as the KKR,[11–14] and TB-LMTO[15] and PAW method[16,17] based on Density Functional Theory, and the numerically tight-binding self-consistent calculation[18] and analytically tight-binding calculation.[19] Some common arguments have been found such as the enhancement of surface magnetism, and the magnetic anisotropy is related to the orbital moment and the spin–orbit coupling interaction (SOC).

The orbital polarization[20,21] can remedy the small orbital moments in the calculations of density functional theory to approach the experimental values, and especially reproduce the correct phase transition in Ce companying with the volume collapses.[21] Besides orbital polarization, the correlation interaction such as the on-site coulomb interaction also enhances the orbital moment.[22] Both orbital polarization and on-site coulomb interaction are localized and play the opposite role to crystal field which quenches the orbital moment to small value in crystal due to the splitting of ground-state energy levels.

However, there are still many contradictions among the already known theoretical results. The density functional calculations with OP (orbital polarization) + SOC (spin–orbit coupling) have given the correct orbital moments, but too large MAE (Magnetic Anisotropy Energy) for tetragonal and cubic Ni. If the OP term switches off, the theoretical values of the magnetic anisotropy energies are close to the experimental values.[23] The magnetic anisotropy energy of CoPt, calculated using the so-called c-RPA[24] is weakly dependent on the new introduced OP interaction and surprisingly consistent with the experiment even only under LSDA approximation without the OP effect.

Based on Brook's theory, the magnetic anisotropy is induced by the spin–orbit interaction.[25] Theoretical works based on Density Functional Theory have also discovered other interesting properties of surface with supported magnetic chains. As in Ref. 17, the authors have studied the magnetism of the ultrathin wires of fifth and sixth row elements supported on Cu(117) and Ag(117) vicinal surfaces. They found that only elements with a half-filled *d*-band are found to have magnetic order on Cu(117) surface; additionally, the ferromagnetic order is energetically stable. On the contrary, on the Ag(117) surface, the antiferromagnetic order is stable. The magnetism of mono-atomic chain is strongly dependent on the local environment absorbed on the surfaces.

Besides the high-index vicinal surfaces such as Ag(117), the reconstructed Au(110)-(1 × 2) surface decorated with one-dimensional troughs along the closed-packed A-[1$\bar{1}$0] direction can be used as a template to grow one-dimensional nanostructure. Experimentally, the distribution of lengths of Ni chains shows that most Ni chains are shorter than 6.[26]

In this work we study the magnetism of mono-atomic Ni chains supported on Au(110)-(1 × 2) surface using the same theoretical method as in Ref. 17. Our studies focus on the magnetic anisotropies of surface-supported magnetic atomic chains. We perform the noncollinear magnetic calculations including the spin–orbit coupling interaction, but without orbital polarization interaction. We have calculated the magnetic anisotropy energies of the supported Ni chains and found off-plane easy magnetization axes perpendicular to the chains and the surface. On the contrary, the easy magnetization axes of the free-standing Ni chains are parallel to these chains. Our results also indicate the close relationship between the magnetic anisotropy and the orbital magnetism.

The paper is arranged as follows. In the next section, we introduce the theoretical method used in this paper. The third section will present the results for single 3d transition metal atoms absorbed on Au(110)-(1 × 2) and Au(111) surfaces. The magnetism of a single magnetic atom on a surface is important to understand the magnetism of materials with more complex structures such as the one-dimensional nanostructure. The reduced dimensionality and coordination number for surface still enhance the magnetism of single absorbed atoms.[27–31] The results of short one-dimensional mono-atomic Ni chains are included in Sec. 4. Finally, we conclude our results.

2. Theoretical Method: Noncollinear Formalism in PAW Method

We have calculated the magnetism of Ni_n (n = 1–5) chains supported on the Au(110)-(1 × 2) surface based on Density Functional Theory[32,33] and the method of Projection of Augmentation Wave (PAW)[34] with the plane-wave base set and Perdew–Burke–Ernzerhof's exchange-correlation potential.[35] The PAW method used in VASP program[36–38] is as accurate as frozen-core all-electron method and hopefully improved to include all-electron relaxation. Our calculations include the noncollinear effects and the spin–orbit coupling which is proved important to heavy metals such as gold. In noncollinear formula, a magnetic moment as a vector can point to any direction in space. The orbital polarization (OP) interaction is not included in our calculations.

The basic theory used in this paper is Hobbs's fully unconstrained noncollinear DFT formulas based on plane wave basis sets and all-electron PAW method.[38,39] Instead of distributing local quantization axis for every atom, which is used in programs based on atom sphere approximation (ASA) or other analogous methods,[40] Hobbs' theory adopts only one global quantization axis, and the vectors of magnetic electronic density are varying smoothly and continuously, which is more suited for the calculations of itinerant magnetism in transition metal materials.

In noncollinear density functional theory,[38–40] the total energy is the functional of a density matrix $n_{\alpha\beta}$, where α and β are the spin indexes along a defined quantization axis. $\alpha = \uparrow$ and $\downarrow$ represent the spin angular momentum point to the positive direction or negative direction of the quantization axis, respectively. The sum of the diagonal elements is the total charge density, that is, $n_{Tr} = \sum_\alpha n_{\alpha\alpha}$. In a noncollinear magnetic system, the off-diagonal elements are nonzero. The 2 × 2 Hermitian matrix can be expanded using the complex matrix basis (I, σ_x, σ_y, σ_z) and expressed as

$$n_{\alpha\beta} = [n_{Tr}\delta_{\alpha\beta} + \mathbf{m}\cdot\boldsymbol{\sigma}_{\alpha\beta}]/2, \tag{1}$$

where $\mathbf{m} = \sum_{\alpha\beta} n_{\beta\alpha}\cdot\boldsymbol{\sigma}_{\alpha\beta}$ is the magnetic electronic density and $\boldsymbol{\sigma}$ is the Pauli matrix. In PAW method, the pseudo-density matrix can be expressed using the pseudo-wave functions as

$$n_{\alpha\beta}(\mathbf{r}) = \sum_n f_n \langle\tilde{\Psi}_n^\beta|\mathbf{r}\rangle\langle\mathbf{r}|\tilde{\Psi}_n^\alpha\rangle, \tag{2}$$

where f_n is the occupation number. The total electronic density matrix $n_{\alpha\beta} = \tilde{n}_{\alpha\beta} + n^1_{\alpha\beta} - \tilde{n}^1_{\alpha\beta}$, where $n^1_{\alpha\beta}$ and $\tilde{n}^1_{\alpha\beta}$ are the on-site electronic density matrixes. The total energy is the sum of three parts $E = \tilde{E} + E^1 - \tilde{E}^1$, where $\tilde{E}$ is smooth functional of the pseudo-density matrix $\tilde{n}_{\alpha\beta}(\mathbf{r})$ evaluated on a regular grid, E^1 and $\tilde{E}^1$ are the functionals of on-site electronic density matrices $n^1_{\alpha\beta}$ and $\tilde{n}^1_{\alpha\beta}$ evaluated on radical support grid around every atom.

The Kohn–Sham Hamilton and Kohn–Sham equations can be obtained from the variation of total energy to the soft pseudo-density matrix and written as

$$H^{\alpha\beta}[n] = -\frac{1}{2}\Delta\delta^{\alpha\beta} + \tilde{v}_{\text{eff}}^{\alpha\beta} + \sum_{(ij)} |\tilde{p}_i\rangle \times (\hat{D}_{ij}^{\alpha\beta} + {}^1D_{ij}^{\alpha\beta} - {}^1\tilde{D}_{ij}^{\alpha\beta})\langle\tilde{p}_j|, \tag{3}$$

$$\sum_\beta H^{\alpha\beta}|\tilde{\Psi}_n^\beta\rangle = \varepsilon_n S^{\alpha\alpha}|\tilde{\Psi}_n^\alpha\rangle,$$

where $S^{\alpha\alpha}$ is the overlapping operator, $\tilde{D}_{ij}^{\alpha\beta}$, ${}^1\hat{D}_{ij}^{\alpha\beta}$, and ${}^1D_{ij}^{\alpha\beta}$ are the nonlocal interactions obtained by the PAW transformation, which are equivalent to the nonlocal pseudo-potential in the ultrasoft-potential method. In noncollinear DFT formulas, the one-electron effective potential $\tilde{v}_{\text{eff}}^{\alpha\beta} = v_H(r)\delta_{\alpha\beta} + v_{xc}(r)\delta_{\alpha\beta} + \mathbf{b}(r)\cdot\boldsymbol{\sigma}^{\alpha\beta}$, which is the summation of electrostatic potential $v_H(r)$, the nonmagnetic part of GGA exchange-correlation correction $v_{xc}(r)$, and the magnetic exchange-correlation potential $\mathbf{b}(r)\cdot\boldsymbol{\sigma}^{\alpha\beta}$, where $\mathbf{b} = \delta E_{xc}/\delta\mathbf{m}(r)$. The magnetic exchange-correlation potential will potentially enhance magnetic moments in noncollinear calculations.

The atoms can have their initial magnetic moments by constructing the magnetic electronic density. The magnetic moments around atoms are equal to their desired values. If an initial magnetic moment points **n** direction, generally the direction of moment changes in Kohn–Sham self-consistent loop. We can use the constrained DFT calculations to fix the direction of the magnetic moment. Our self-consistent calculations show that the directions of magnetic moments change very less in ferromagnetic materials although using the unconstrained DFT

calculations shown in Table 2. In real ferromagnetic materials, the directions of magnetic moments are hard to change, once the magnetic domains have formed. This is because the change of magnetization direction must include the changes of magnetic moments of all magnetic atoms in the materials. We can add an external magnetic field to change the directions of magnetic moments. Of course, there exists an easy magnetization axis which is stable direction of magnetic moments. We need the "strongest" magnetic field to change directions of magnetic moments away from the direction of the easy magnetization axis. However, for the materials with more complex magnetic structures such as the canted and spiral magnetic structures, the relaxations of directions of magnetic moments are intrinsic, and the use of unconstrained DFT is essentially important.[38,39]

3. The Magnetism of 3d Transition Metal Atoms Absorbed on Au(110)-(1 × 2) and Au(111) Surface

The missing row Au(110) surface reconstructs from Au(110) surface by having missed closed-packed Au chains every others. The troughs along the close-packed A-[1$\bar{1}$0] direction are formed. We construct a crystal slab with four atomic layers including 28 gold atoms. At the first step, we optimized the lattice constant of gold crystal which is about 4.2 Å. In the procession of optimization, the RMM-DIIS algorithm[36] is used in the total-energy minimum with plane-wave energy cutoff 229.9 eV and the 6 × 6 × 6 Monkhorst–Pack K-points mesh. The size of super-cell is 11.8 Å × 8.4 Å × 5.94 Å.

We add a vacuum layer by extending the super-cell along the C-[110] direction. The size along the C-[110] direction of super-cell including vacuum layer is equal to 16 Å. The lattice constant of surface is generally smaller than that of the crystal. Thus, we optimized the slab with vacuum layer together. Based on the optimized lattice constant, the size of the super-cell is 11.523 Å × 8.148 Å × 15.52 Å. The vacuum layer is about twice thicker than the thickness of the slab. For the optimized Au(111) surface, the size of super-cell is about 11.5 Å × 9.97 Å × 20 Å including 64 gold atoms. In the above optimizations, we only change the lattice constant. The initial

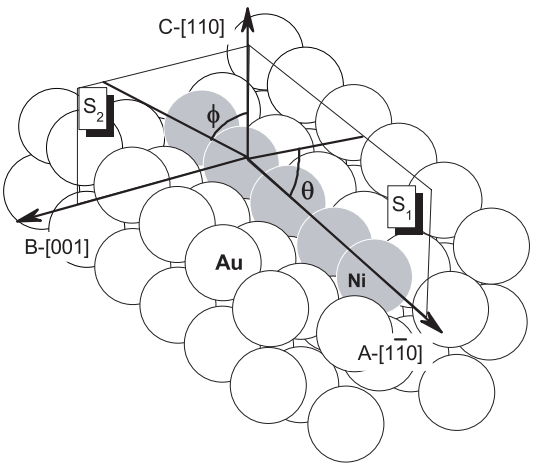

Fig. 1. The schematic diagram of an atomic chain supported on the Au(110)-(1 × 2) surface. The trough of the reconstructed surface is along the A-[1$\bar{1}$0] direction. The gray spheres are the absorbed atoms in the trough. The white spheres are the Au atoms of the surface. The plane including both C-[110] axis and A-[1$\bar{1}$0] axis is named as S_1, the plane including both C-[110] axis and B-[001] axis as S_2. The rotating angle of any vector in S_1 to A-[1$\bar{1}$0] axis is labeled as θ, and the rotating angle of any vector in S_2 to C-[110] axis is labeled as ϕ.

structures are constructed by placing the 3d transition metal atoms on the hollow sites of the Au(111) and Au(110)-(1 × 2) surface in the trough (Fig. 1). The initial structures are optimized for all atoms except for the bottom atoms by having used the conjugate-gradient method. The K-point meshes of 2 × 2 × 1 and Γ points are used to sample the first Brillouin-zone in the corresponding calculations of the electronic structures for Au(110)-(1 × 2) and Au(111) surfaces, respectively.

We use both collinear and noncollinear density functional calculations, but mainly present the non-collinear results. In noncollinear DFT calculations, we use the optimized structures from collinear DFT calculations. Based on the relaxed structures, we calculate more exactly the electronic structures using the RMM-DIIS algorithm[36] with the (6 × 6 × 1) Monkhorst–Pack grids sampling the first Brillouin zone. The criterion of convergence for total energy is 0.0001 eV. The Methfessel–Paxton smearing width is equal to 0.20 eV. The energy cutoffs for plane wave are different for different species of atom which are summarized in Table 1. The magnetic moment for a single atom is calculated by considering the electrons in a Wigner-Seitz sphere centered at the position

Table 1. The Wigner Seitz Radii (WSR Å) and Energy-Cutoff of plane wave (Ecut eV) for 3d transition-metal atoms and Au atom.

	Ti	V	Cr	Mn	Fe	Co	Ni	Cu	Au
WSR	1.323	1.323	1.323	1.323	1.302	1.302	1.286	1.312	1.503
Ecut	178.4	192.6	227.1	269.9	267.9	268.0	269.6	273.2	229.9

of the atom. The Wigner Seitz Radii for 3d transition metal atoms are also summarized in Table 1. We choose the C-[110] direction as the quantization axis. We emphasize the influence of surface deformation on the orbital moments of the absorbed atoms. The orbital polarization interaction is omitted in this work but the spin–orbit coupling interaction is included. We obtain smaller orbital moments compared with the pervious density functional calculations including the orbital polarization interaction.[43]

3.1. *The influence of structural relaxations on the magnetism of a single absorbed 3d transition atom*

If we want to know the direction of magnetic moment relative to the surface, we should use the noncollinear DFT formulas. At the first step, we calculate the magnetic moments of the absorbed 3d atoms on the Au(110)-(1 × 2) and Au(111) surfaces including the spin–orbit coupling interactions. From Fig. 2, we can see that the spin moments reach the maximum in the middle of the group. The directions of magnetic moments for 3d atom studied in this work are all along the C-[110] direction after self-consistent calculations. The large spin moment of the absorbed Mn atom is about $4.163\,\mu_B$ on the Au(110)-(1 × 2) surface. The change of magnetic moments per absorbed magnetic atom across the 3d row has been found in many other *ab initio* calculations such as 3d atoms on Au(001), Ag(001)[41] and Cu(001)[42] surfaces. Our results are consistent very well with these results.

Both the electronic correlation and the crystal field have significant influence on the orbital moments of the absorbed 3d atoms. If the electronic correlation is stronger than the crystal field, the orbital moment is large, otherwise small. The absorbed Ti, V, and Co atoms have visible orbital moments $0.086\,\mu_B$, $0.082\,\mu_B$, and $0.092\,\mu_B$ on the

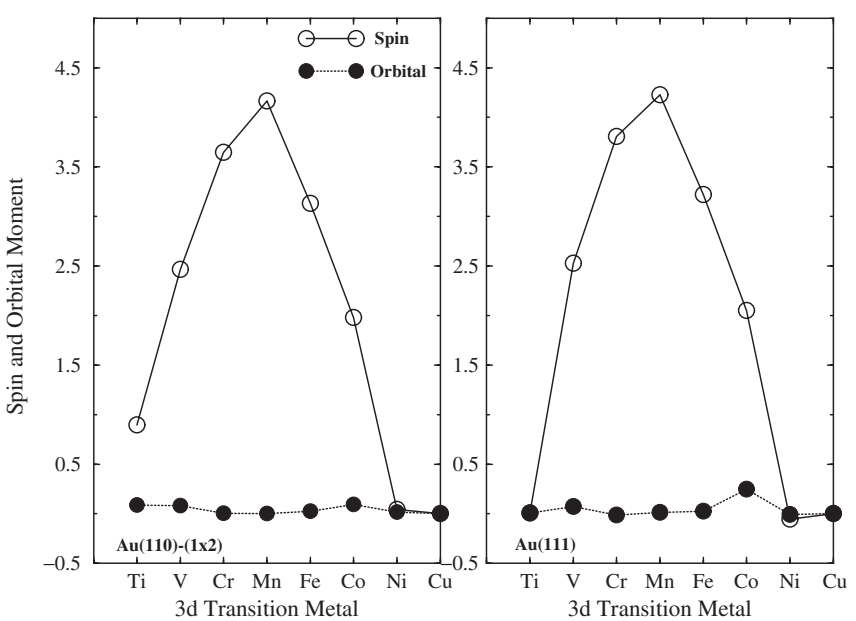

Fig. 2. The spin (solid lines) and orbital (dot lines) moments (μ_B) of the absorbed 3d atoms. The left panel shows the results for Au(110)-(1 × 2) surface, the right panel for the Au(111) surface.

Au(110)-(1 × 2) surface, and $0.006\,\mu_B$, $0.071\,\mu_B$, and $0.247\,\mu_B$ on the Au(111) surface, respectively. Cabria *et al.* obtained larger orbital moments (about $0.5\,\mu_B$) of Fe and Co atoms absorbed on Au(001) surface using the spin polarization relativistic KKR method including the orbital polarization term.[41,43] The usual exchange-correlation potentials (LDA or GGA) underestimate the electronic correlations such as the Coulomb correlation and the orbital polarization; thus, the obtained orbital moments in this work are generally small compared with the experimental values[20–22,43] although our work includes the spin–orbit coupling interaction. The small values of orbital moments of the absorbed Cr atoms in our calculations are not related to the crystal field but to its electronic structure. In the individual Cr atom, five 3d electrons half-fill the 3d states, and the total orbital moment is very small.

The coordination numbers of surface atoms and surface-supporting atoms are generally smaller than those in bulk. So, the magnetism of surface is generally stronger than that in bulk. The supported atoms on the surface have possibly larger magnetic moments. The lack of the orbital polarization is not the obstacle to study the structural influence on the orbital moment. In order to clearly illustrate the effects of the crystal deformations (or the cubic distortions), we compare the results on the deformed surface with the prefect Au(110)-(1 × 2) surface. The absorbed 3d atoms on the prefect surface still modify their positions to reach their stable positions, while the surface atoms are fixed. We find from Fig. 3 that, except for V and Ti atoms, the surface relaxations generally quench the orbital moments of the other absorbed 3d atoms. The changes of the orbital moments in response to the relaxations are closely related to the changes of the depth of the 3d atoms embedded in the trough of the reconstructed Au(110) surface. The absorbed atoms are deeper in the trough, and their orbital moments are quenched to smaller values due to the stronger crystal field. The absorbed V and Ti atoms rise above or with the same height with the top row of the trough after the relaxations, so that their orbital moments enhance, which oppose the orbital quenching for the other 3d atoms. This is due to the weaker crystal field above the surface than that in the trough.

The 3d density of states of the absorbed 3d atoms on the two surfaces are shown in Fig. 4. Our results show that the 3d densities of states at Fermi-energies

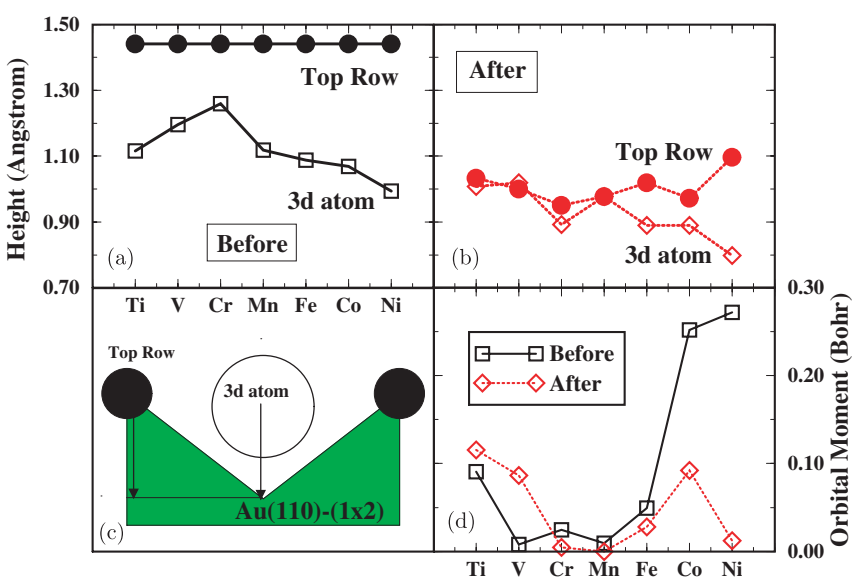

Fig. 3. The effects of structure-relaxation on orbital moments of the absorbed 3d transition metal atoms: (a) The heights of top-row and absorbed 3d atoms before the full-structure relaxations. The stable positions are different for different 3d atoms, which are obtained by the single-atom optimizations on the unrelaxed surface; (b) the heights of top row and absorbed 3d atoms after having done full-structure relaxations. The V atom is higher above the top row after the full-relaxation; (c) the schematic figure defines the heights of top row and absorbed atoms using two arrows pointing to the bottom of the trough; (d) the changes of orbital moments before and after the full-relaxations.

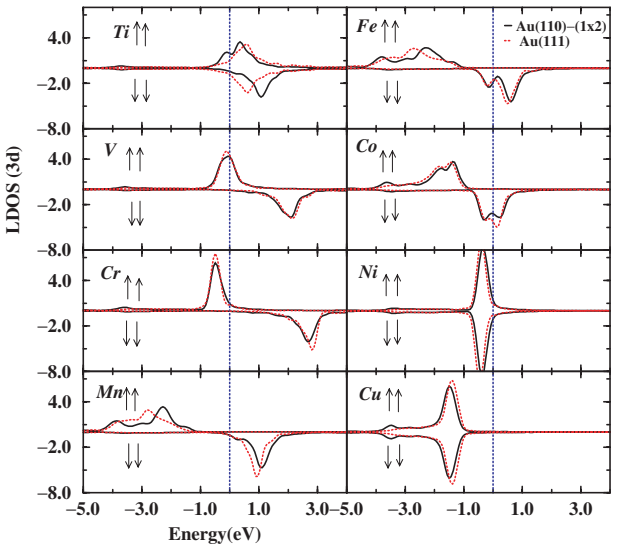

Fig. 4. The 3d densities of state (DOS) for the 3d atoms absorbed on the Au(110)-(1×2) (solid lines) and Au(111) (dot lines) surfaces.

are closely related to the orbital moments of the absorbed 3d atoms. The absorbed Ti, V, and Co atoms on the Au(110)-(1 × 2) surface and V, Co atoms on the Au(111) surface have large 3d densities of states at the Fermi-energies and large orbital moments too. We get the same arguments on the magnetism of Ni_n (n = 1–5) chains. Large density of state $N(E_f)$ at Fermi-energy is advantaged to the formation of the orbital moment as well as the spin moment. The single Ni atom has small magnetic moment; however, we can see in the next section that the Ni clusters such as one-dimensional Ni chains have significant magnetic moments on the Au surface. The exchange interactions between Ni atoms prevent the decay of magnetic moments of Ni atoms.

4. The Magnetism of Ni Atomic Chains

The initial Ni chains are located in the trough along the A-[1$\bar{1}$0] direction with the nearest-nearby distance of Ni atoms about 2.88 Å that is the same as the nearest-nearby distance of Au atoms in the missing Au chain (Fig. 1). The surface slab includes four atomic layers with 56 Au atoms and the size of the super-cell is 23.046 Å × 8.148 Å × 15.52 Å. We have relaxed the initial structures using the conjugate-gradient method. The 2 × 2 × 1 K-point mesh is used to sample the Brillouin-zone in the corresponding electronic-structure calculations. Based on the relaxed structures, we calculated their electronic structures more exactly using RMM-DIIS algorithm with the (4 × 4 × 1) Monkhorst–Pack grids sampling the first Brillouin zone. The other information is the same as in the calculation for single 3d atom.

We have also calculated the magnetism of free-standing Ni chains by removing all surface atoms but still preserving in the same box cell. There are mirror atomic chains, because of periodic boundary conditions along three directions. The interactions of free-standing chains with their mirror atomic chains are small and negligible if the box cell is large enough. We have only chosen short chains, Ni_n, where n is less than 6 and large box is size of 23 Å along the direction parallel to the chains so that the ends of chains are far away from the boundaries of the box cell. The Ni_n atomic chains in the trough of Au(110)-(1 × 2) surface are straight lines. As we optimize the structures of free-standing chains, all atoms are only allowed to modify their positions along the direction of chains, and the optimized free-standing Ni chains still keep straight line shape. We try to compare the results of surface-support straight chains with those of free-standing straight chains. The quantization axis is still along the C-[110] direction in this section.

4.1. *Magnetism of Ni_n (n = 1–5)*

All Ni atoms in the cell have their initial magnetic moments in our calculations. We calculate the total energies, the spin and orbital magnetic moments of the supported Ni chains when they are magnetized along the A-[1$\bar{1}$0] direction parallel to the chains or C-[110] direction perpendicular to the chains, respectively. The magnetization of an atomic chain in study paper means that the magnetic moments for every Ni atom align along the same direction. The values of initial moments of Ni atoms are all the same; however, the values after the self-consistent calculations are probably not the same for all Ni atoms. The orientations of magnetic moment may be manually changed to simulate the different magnetizing directions. In a single self-consistent calculation, the directions of magnetic moments change very small for the ferromagnetic Ni chains although we have

Table 2. The spin and orbital magnetic moments (Bohr) for atoms of Ni_5 chain when the magnetization directions are along the A-[1$\bar{1}$0], B-[001], and C-[110], respectively.

	A-[1$\bar{1}$0]			B-[001]			C-[110]		
	M_A	M_B	M_C	M_A	M_B	M_C	M_A	M_B	M_C
Ni(1)	0.434	0.0	−0.006	0.0	0.411	0.0	0.017	0.0	0.430
Ni(2)	0.449	0.0	0.006	0.0	0.426	0.0	−0.012	0.0	0.449
Ni(3)	0.352	0.0	0.000	0.0	0.323	0.0	0.001	0.0	0.366
Ni(4)	0.449	0.0	−0.007	0.0	0.452	0.0	0.015	0.0	0.452
Ni(5)	0.437	0.0	0.005	0.0	0.446	0.0	−0.015	0.0	0.432
	L_A	L_B	L_C	L_A	L_B	L_C	L_A	L_B	L_C
Ni(1)	0.105	0.0	0.000	0.0	−0.085	0.0	0.009	0.0	0.080
Ni(2)	0.097	0.0	−0.010	0.0	−0.082	0.0	−0.012	0.0	0.093
Ni(3)	0.092	0.0	0.000	0.0	−0.065	0.0	0.001	0.0	0.060
Ni(4)	0.097	0.0	0.010	0.0	−0.088	0.0	−0.012	0.0	0.096
Ni(5)	0.105	0.0	−0.001	0.0	−0.092	0.0	−0.009	0.0	0.079

used the unconstrained Density Functional calculations (Table 2).

The chains become short after the relaxations and, the average nearest-nearby distance of Ni atoms in Ni_5 chain is about 2.75 Å shorter than 2.88 Å that in the initial structure, shown in Fig. 1. We choose two magnetizing directions: A-[1$\bar{1}$0] direction parallel to the chains and C-[110] direction perpendicular to the chains. The size-dependent magnetic moments are shown in Fig. 5(a). From this figure we can see that the spin moments of single absorbed Ni atom are small, $0.147\,\mu_B$, for the magnetization along the C-[110] direction and $0.127\,\mu_B$ for the A-[1$\bar{1}$0] direction. The spin moments per atom of the Ni_2 chain increase to $0.455\,\mu_B$ for A-[1$\bar{1}$0] direction and $0.464\,\mu_B$ for the C-[110] direction. The spin moments of Ni_3 have a slight decrease for C-[110] direction but large decrease for the A-[1$\bar{1}$0] direction. The spin moments decrease slightly and try to keep constant as the chain lengths increase above 4. Our results show that the spin moments of Ni atoms on the reconstructed Au(110) surface are smaller than the value $0.675\,\mu_B$ in crystal Ni having been calculated using the same method in our work.

The magnetic order is an important aspect of material magnetism. Experimentally, the long ferromagnetic order is found for Co chains stabilized above a finite temperature on the Pt(997) surface.[5] When increasing temperature higher than

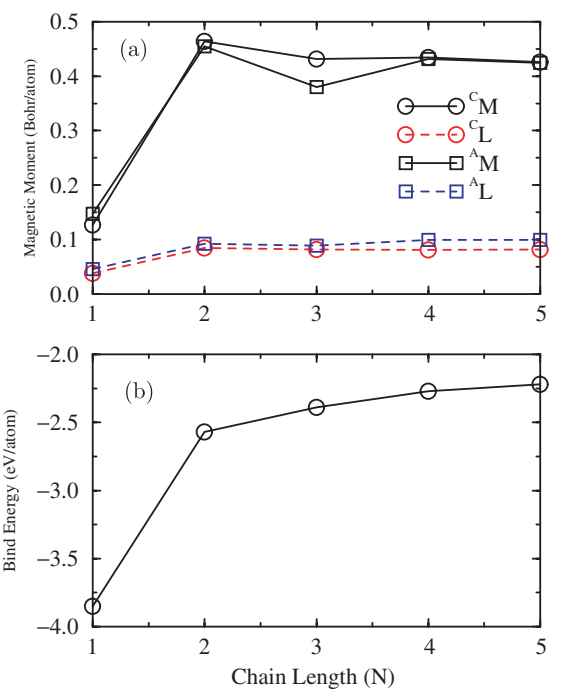

Fig. 5. (a) The spin ^{A}M, ^{C}M and orbital ^{A}L, ^{C}L moments change with the length of Ni chains. The ^{A}M and ^{C}M do not present the A and C components of the spin moment **M**. They present the spin magnetic moments when the magnetizations along the A-[1$\bar{1}$0] and C-[110] directions are obtained from different self-consistent calculations. ^{A}L and ^{C}L have the same meaning for orbital moments. (b) Interaction energies between the Ni chains and the surface. The larger absolute values indicate the stronger interaction with the surface.

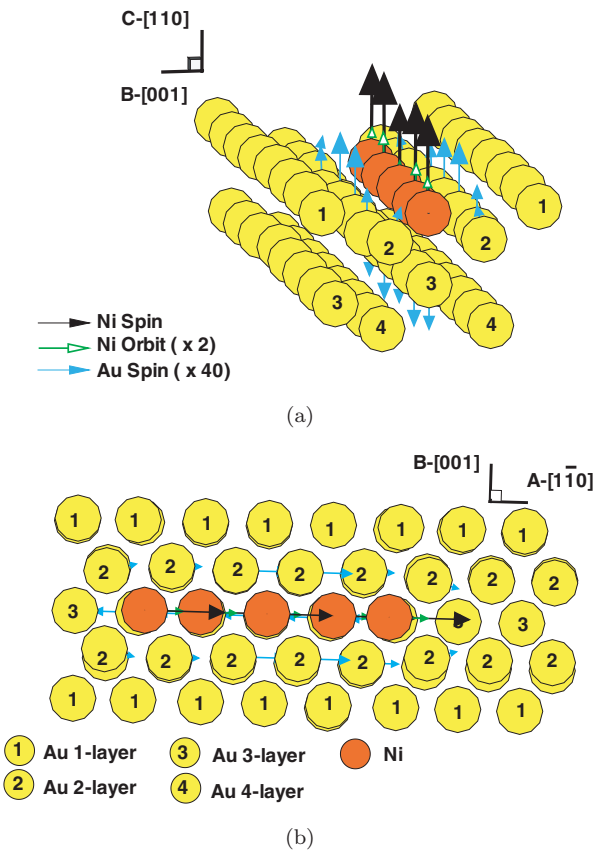

Fig. 6. The vector graphs of the spin magnetic moments of the Ni chain which illustrate the ferromagnetic order of the Ni_5 chain based on our calculations. (a) and (b) correspond to the magnetizations along the C-[110] and A-[1$\bar{1}$0] directions, respectively. The smaller spin magnetic moments of Au atoms and the orbital magnetic moments of Ni atoms are amplified 40 times and 2 times, respectively to show them with the larger spin moments of Ni atoms together in the same figure clearly.

the normal temperature, the long ferromagnetic order is destroyed and changes into short ferromagnetic fragments. In our calculations, the short Ni chains are ferromagnetic. Figure 6 shows the ferromagnetic order of the surface-supported Ni_5 chains for the magnetization for C-[110] and A-[1$\bar{1}$0] directions. The spin-polarizations of surface Gold atoms near the Ni chain are induced by the magnetic Ni atoms, which almost disappear for Gold atoms far from the Ni chain. The spin magnetic moments for the Gold atoms near the Ni chain are parallel to the magnetic moments of the Ni chain. The spin moments of the 3-layer Gold atoms are anti-parallel to the magnetic moments of Ni chain, because the 3-layer Gold atoms are near the bottom of the slab where there is another surface. The surface effects lead the spin moments of the Gold atoms on the surface point outward. We have also calculated the antiferromagnetic configurations, nonmagnetic configurations, and other noncollinear magnetic configurations, and found their energies higher than that of the ferromagnetic configurations. Thus, our calculations show that the Ni chains with ferromagnetic order are most energetically favorable. It is interesting to find from Fig. 5 that, when magnetizing the Ni chains parallel to the chain, the orbital moments are larger than those perpendicular to the chains. The spin moments for every Ni atom of the ferromagnetic Ni chain almost do not change their directions after the Kohn–Sham self-consistent calculations for all three magnetization directions (Table 2). The spin moment of the middle atom, smaller than that of other atoms shows that the short Ni_5 chain is not in prefect ferromagnetic order.

The interaction between supported Ni_n chain and surface can be measured with the interaction energy $E_I = E^{\text{tot}} - E^s - E^f$, where E^{tot} is the total energy, E^s is the energy of slab with relaxed surface, and E^f is the energy of free-standing chain. Figure 5(b) shows that the interaction energies (per atom) between Ni chain and the surface increase with the chain lengths. These results indicate that short Ni chains are more energetically favorable on Au(110)-(1×2) surface at low coverage of Ni atoms. This is consistent with the experiments[26] in which most of the Ni chains are shorter than 6. From Fig. 7, we can see that the densities of states of 3d states of Ni_5 chain change very small when the magnetization changes from the C-[110] direction to the A-[1$\bar{1}$0] direction. The spin magnetic moments do also change very small (Fig. 5). From Fig. 5, the changes of orbital moments are more significant when the magnetizing directions change. Although the orbital moments are underestimated due to the absence of (OP) orbital polarization term, our results still show that magnetic anisotropy is closely related to the orbital degree of freedom. For compact magnetic islands on metal surface such as Co/Pt(111),[44] the orbital moments per atom decrease with increasing island sizes. This is because only atoms at the edge of the island have significant contributions to the total orbital moments. However, for one-dimensional island, all atoms have significant contribution to the total orbital moments. The orbital moments

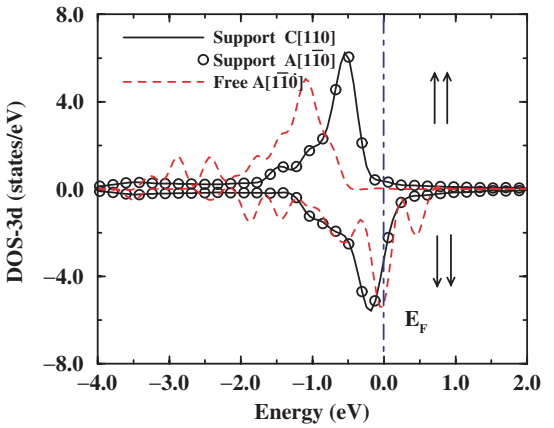

Fig. 7. The projected DOS of 3d states of the supported Ni_5 chain along different magnetization directions when the chain is magnetized along these different directions, respectively (the solid lines for the C-[110] direction and the circles for the A-[1$\bar{1}$0] direction). The spin-up (or spin-down) means along the positive (or negative) direction of two magnetization directions. The dash-line is the DOS for free-standing Ni chain when magnetizing it along the A-[1$\bar{1}$0] direction.

per atom keep constant as the lengths of chains beyond 4.

4.2. *The magnetic anisotropy of Ni_5 chain*

In the above subsection, we have chosen two magnetization directions, A-[1$\bar{1}$0] and C-[110]. In this subsection, we study the magnetic anisotropy of the Ni_5 chain and show that C-[110] direction is along the easy magnetization axis. The magnetic anisotropy energies in S_1 and S_2 planes are defined as $\delta E_1 = E^C - E^A$ and $\delta E_2 = E^C - E^B$, respectively. E^A, E^B, and E^C are the total energies when magnetizing the chain along the A-[1$\bar{1}$0] ($\theta = 0°$), B-[001] ($\phi = 0°$), and C-[110] ($\theta = 90°$) directions, respectively. The magnetic anisotropy of one-dimensional structure is more prominent than compact structures such as surface and bulk. Figure 8 shows how the total energies, the spin and orbital moments change with two magnetization angles in the above two planes. We

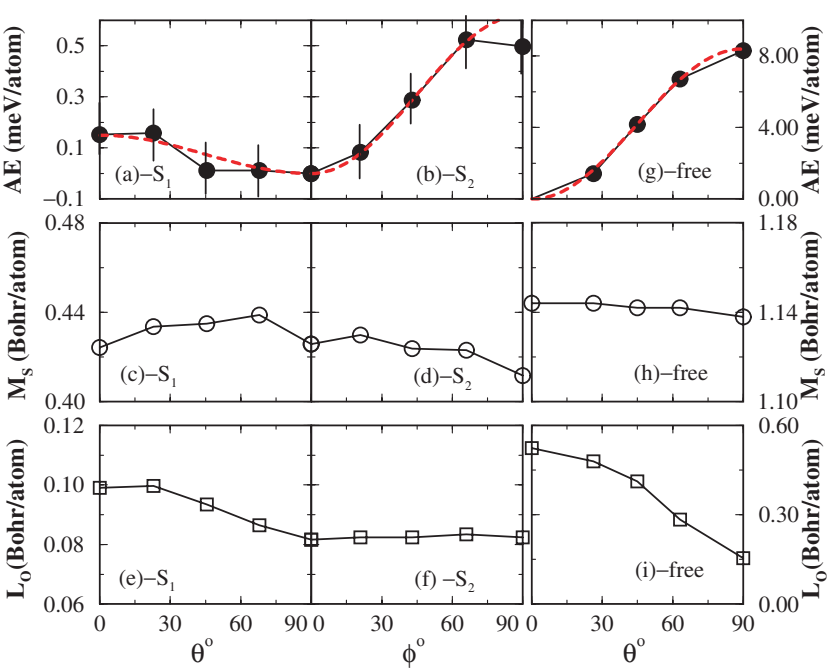

Fig. 8. The anisotropy energies (a, b), the spin (c, d), and orbital moments (e, f) of the supported Ni_5 chain change with the magnetization angles θ and ϕ in the planes S_1 and S_2 defined above. The easy magnetization direction is perpendicular to the surface with $\theta = 90°$ and $\phi = 0°$. The anisotropy energies (g), spin moments (h), and orbital moments (i) of the free-standing Ni_5 chain change with the magnetization angles θ in the planes S_1. The easy magnetization direction is parallel to the chain with $\theta = 0°$. Error bars in (a, b) represent the lowest limit of allowed error in the total energy of about ± 0.1 meV. The magnetic anisotropy energy curves are fitted using function $K_0 + K_1 \sin^2(\theta)$ for (a,g) and $K_0 + K_1 \sin^2(\phi)$ for (b)(red dash-lines).

find from Figs. 8(a) and 8(b) that there is weak magnetic anisotropy in the S_1 plane and relatively strong magnetic anisotropy in the S_2 plane. The magnetic anisotropy energies are 0.158 meV/atom and 0.524 meV/atom, respectively in the two planes. The shape anisotropy determines the large difference of magnetic anisotropy energy in the two planes because of one-dimensional characteristic of monoatomic chain. In the same plane such as the plane S_1, the magnetic anisotropy is determined by spin–orbit coupling. The easy magnetization directions in both the S_1 and S_2 planes are all along the C-[110] direction ($\theta = 90°$ and $\phi = 0°$), which is perpendicular to the chain and the surface. The magnetic anisotropy energies can be represented as $K_0 + K_1 \sin^2(\theta)$ in the S_1 plane and $K_0' + K_1' \sin^2(\phi)$ in the S_2 plane.[45,25] The parameters $K_0 = 0.158$ meV, $K_1 = -0.158$ meV in S_1 and $K_0' = 0.0$ meV, $K_1' = 0.62$ meV in S_2 are obtained by fitting the magnetic anisotropy curves using the above two functions. The magnetic anisotropy is not good fit with $K_0 + K_1 \sin^2(\theta)$ in S_1. The underlying reasons are (1) there is not simple cubic symmetry in the region where the one-dimensional atomic chain is absorbed; (2) the heterogeneously distributed nearest-nearby distances are along the chain induced by the lattice misfit between the chain and the substrate. On the other hand, the value of K_1 is close to the lowest limit of allowed error in total energy about ± 0.1 meV; thus, more accurate calculations are required.

Experimentally, the values of magnetic anisotropy energies are from 1 meV to 10 meV for magnetic clusters, and from 0.1 meV to 1.0 meV for magnetic films on the metal surface. Based on our calculations, the magnetic anisotropy energies for Ni chains on the reconstructed Au(110) surface are close to the values of the magnetic film. This is because the atoms on the Ni chain replace the atoms of the first layer of the original surface and have almost the same coordinate number in their monolayer film. The experiment in Co/Pt(997) had shown that the anisotropy energies were about 2 meV for the monatomic Co chains and 0.14 meV for the monolayer Co film on the Pt(997) surface.[5] From Fig. 8(e) we find that the orbital moments reach the minimum when magnetizing the Ni chain along the easy magnetization direction. The orbital moments almost keep constant when the magnetization angle ϕ changes in the S_2 plane shown in Fig. 8(f). The directions of orbital moments for every Ni atom on the chain are almost parallel to their spin moments when the magnetizations are along the A-[1$\bar{1}$0] and C-[110] axes, however, anti-parallel to their spin moments for the magnetization along the B-[001] axis shown in Table 2. It is most energetically unfavorable when the spin moment of the Ni chain points to the B-[001] direction ($\phi = 90°$) from the curve of magnetic anisotropy energy in the S_2 plane (Fig. 8(b)).

4.3. *The magnetic anisotropy of free-standing Ni_5 chain and discussion*

In order to illustrate the surface influence on the magnetic anisotropy, as a comparison, we also calculate the magnetic anisotropy of free-standing Ni_5 chain in the same box. All calculating details are the same as those of the surface-supported Ni_5 chain except for removing the surface atoms. The average nearest-neighbor distance of Ni atoms is about 2.196 Å shorter than 2.77 Å for the surface-support Ni_5 chain and 2.5 Å in Ni crystal. The changes of densities of states of 3d states for free-standing Ni chain are that the majority spin-up densities of states are far from to the Fermi-energy. The larger densities of states at Fermi-energy contributed by the minority spin-down DOS indicate that there are larger spin and orbital moment magnetic moments for free-standing Ni chain.

We only consider the changes of the total energies with the angle θ. From Fig. 8(g), we can see that the easy magnetization direction is now parallel to the chain which is different from perpendicular to the chain for the surface-supported Ni_5 chain. For free-standing chain we find $K_0 = 0.0$ meV and $K_1 = 8.4$ meV in S_1. The anisotropy energy is large compared with the surface-supported Ni_5 chain. The change of the sign of K_1 compared with the surface-supported chain means that the easy magnetization axis changes in the S_1 plane. The change of the easy magnetization axis had been found in other theoretical works such as Co chains on Pd(110) surface.[18] Experimentally, the changes of easy magnetization axis were found in the growth of magnetic film on metal surface when the thickness of film is beyond a critical value d_c. The transitions from in-pane to

perpendicular plane for Ni/Cu(001)[46] and inversely from perpendicular to in-plane for Fe/Ag(100)[47] and Co/Au(111)[48] were found at critical coverage about 5–7 ML. The transitions are close related with the transitions from films with heterogeneously distributed strains to films with homogenously distributed strains once beyond critical thickness. The atomic chains in this work are found in an initial stage of film growth and have the easy magnetization axis perpendicular to the surface.

The spin moments keep almost constant when the magnetization angle changes from $\theta = 0°$ to $\theta = 90°$. The spin moment about $1.14\,\mu_B$ per atom is significantly large than its values in Ni crystal, $0.675\,\mu_B$. The behavior of the orbital moment is similar to the surface-supported Ni_5 chain, that is, reaches the minimum when perpendicularly magnetizing the chain. The underlying reason is geometric, that is, the orbital currents (or Molecular Currents) of neighbor atoms have large overlapping, and their cancellations are also large which is disadvantageous to form larger orbital moments. The values of orbital moments from $0.2\,\mu_B$ to $0.6\,\mu_B$ are larger than one power of the values of the surface-supported Ni atoms. The easy magnetization axis of free-standing Ni chain A-$[1\bar{1}0]$ is different from the easy magnetization axis of surface-supported chain C-[110].

5. Conclusion

Based on the Density Functional Theory, we have calculated the magnetic anisotropies of the surface-supported and free-standing Ni chains. The easy magnetization axis of the supported Ni chain is perpendicular to the chain and the surface, but parallel to the chain for free-standing chain. The difference of the easy magnetization axes for the surface-supported chain and free-standing chain is also found in density functional calculations of other system. Our results indicate the intrinsic relationship between the magnetic anisotropy and the orbital moment of the Ni chains. In the environments of the crystal, the orbital moment is generally quenched to small value due to the energy-level splitting induced by the crystal field. Compared with the spin moment, orbital moment is more sensitive to the change of magnetization direction. The orbital quenching is dependent on the magnetized directions. The magnetic anisotropy of materials is determined both by the orbital quenching and spin–orbit coupling. For a single absorbed atom, the surface relaxations generally deform the surface and modify the position of the absorbed atom. If the relaxations lift the absorbed atom out of the trough on the reconstructed Au(110) surface, the orbital moment enhances due to weaker crystal fields, and if the relaxations make the absorbed atom deeply embedded in the trough the orbital moment quenches to smaller value due to the stronger crystal field.

Acknowledgments

One of the authors (W. Fan) is greatly indebted to Prof. Q. Q. Zheng, Dr J. L. Wang, Prof. L. J. Zou, and Prof. Z. Zeng for their helpful discussions. This work had been run on computers in the Center for Computational Science, Hefei Institutes of Physical Science, and on LSSC in the Institute of Computational Mathematics and Scientific/Engineering Computing, Chinese Academy of Sciences. X. G. Gong is additionally supported by the National Science Foundation of China, the special funds for major state basic research.

References

1. H. J. Elmers, J. Hauschild, H. Höche, U. Gradmann, H. Bethge, D. Heuer and U. Köhler, *Phys. Rev. Lett.* **73** (1994) 898.
2. J. Shen, R. Skomski, M. Klaua, H. Jenniches, S. S. Manoharan and J. Kirschner, *Phys. Rev. B* **56** (1997) 2340.
3. J. Hauschild, H. J. Elmers and U. Gradmann, *Phys. Rev. B* **57** (1998) R677.
4. M. Pratzer, H. J. Elmers, M. Bode, O. Pietzsch, A. Kubetzka and R. Wiesendanger, *Phys. Rev. Lett.* **87** (2001) 127201.
5. P. Gambardella, A. Dallmeyer, K. Maiti, M. C. Malagoli, W. Eberdardt, K. Kern and C. Carbone, *Nature (London)* **416** (2002) 301.
6. P. Gambardella, M. Blanc, L. Bürgi, K. Kuhnke and K. Kern, *Surf. Sci.* **449** (2000) 93.
7. P. Gambardella, M. Blanc, K. Kuhnke and K. Kern, *Phys. Rev. B* **61** (2000) 2254.
8. D. Li, C. Yu, J. Pearson and S. D. Bader, *Phys. Rev. B* **66** (2002) 020404.
9. C. Boeglin, S. Stanescu, J. P. Deville, P. Ohresser and N. B. Brookes, *Phys. Rev. B* **66** (2002) 014439.
10. H. Dreyssé and C. Demangeat, *Surf. Sci. Rep.* **28** (1997) 65.
11. V. Bellini, N. Papanikolaou, R. Zeller and P. H. Dederichs, *Phys. Rev. B* **64** (2001) 094403.

12. K. Wildberger, V. S. Stepanyuk, P. Lang, R. Zeller and P. H. Dederichs, *Phys. Rev. Lett.* **75** (1995) 509.
13. B. Lazarovits, L. Szunyogh, P. Weinberger and B. Uj́falussy, *Phys. Rev. B* **68** (2003) 024433.
14. M. Eisenbach, B. L. Györffy, G. M. Stocks and B. Újfalussy, *Phys. Rev. B* **65** (2002) 144424.
15. M. Komelj, C. Ederer, J. W. Davenport and M. Fähnle, *Phys. Rev. B* **66** (2002) 140407.
16. D. Spišák and J. Hafner, *Phys. Rev. B* **65** (2002) 235405.
17. D. Spišák and J. Hafner, *Phys. Rev. B* **67** (2003) 214416.
18. J. Dorantes-Dávila and G. M. Pastor, *Phys. Rev. Lett.* **81** (1998) 208.
19. R. Druzinic and W. Hübner, *Phys. Rev. B* **55** (1997) 347.
20. M. S. S. Brooks and P. J. Kelly, *Phys. Rev. Lett.* **51** (1983) 1708.
21. O. Eriksson, M. S. S. Brooks and B. Johansson, *Phys. Rev. B* **41** (1990) 7311.
22. I. V. Solovyev, A. I. Liechtenstein and K. Terakura, *Phys. Rev. Lett.* **80** (1998) 5758.
23. O. Hjortstarm, K. Baberschke, J. M. Wills, B. Johansson and O. Eriksson, *Phys. Rev. B* **55** (1997) 15026.
24. I. V. Solovyev, *Phys. Rev. Lett.* **95** (2005) 267205.
25. H. Brooks, *Phys. Rev.* **58** (1940) 909.
26. A. Hitzke, M. B. Hugenschmidt and R. J. Behm, *Surf. Sci.* **389** (1997) 8.
27. K. D. Gross, D. Riegel and R. Zeller, *Phys. Rev. Lett.* **63** (1989) 1176.
28. K. D. Gross, D. Riegel and R. Zeller, *Phys. Rev. Lett.* **65** (1990) 3044.
29. M. C. Hanf, C. Pirri, J. C. Peruchetti, D. Bolmont and G. Gewinner, *Phys. Rev. B* **36** (1987) 4487.
30. D. Riegel, L. Büermann, K. D. Gross, M. Luszik-Bhadra and S. N. Mishra, *Phys. Rev. Lett.* **62** (1989) 316.
31. J. E. Ortega and F. J. Himpsel, *Phys. Rev. B* **47** (1993) 16441.
32. P. Hohenberg and W. Kohn, *Phys. Rev.* **136** (1964) B864.
33. W. Kohn and L. J. Sham, *Phys. Rev.* **140** (1965) A1133.
34. P. E. Blöchl, *Phys. Rev. B* **50** (1994) 17953.
35. J. P. Perdew, K. Burke and M. Ernzerhof, *Phys. Rev. Lett.* **77** (1996) 3865.
36. G. Kresse and J. Furthmuller, *Comput. Mater. Sci.* **6** (1996) 15.
37. G. Kresse and D. Joubert, *Phys. Rev. B* **59** (1999) 1758.
38. D. Hobbs, G. Kesse and J. Hafner, *Phys. Rev. B* **62** (2000) 11556; M. Marsman, *Magnetism*, the talks and hands-on sessions of VASP Workshop, Vienna (2003).
39. D. Hobbs, J. Hafner and D. Spišák, *Phys. Rev. B* **68** (2003) 014407.
40. L. M. Sandratskii, *Adv. Phys.* **47** (1998) 91.
41. I. Cabria, B. Noas, R. Zeller and P. H. Dederichs, *Phys. Rev. B* **65** (2002) 054414.
42. V. S. Stepanyuk, A. N. Baranov, W. Hergert and P. Bruno, *Phys. Rev. B* **68** (2003) 205422.
43. B. Nonas, I. Cabria, R. Zeller, P. H. Dederichs, T. Huhne and H. Ebert, *Phys. Rev. Lett.* **86** (2001) 2146.
44. P. Gambardella, S. Ruspoi, T. Cren, N. Weiss, and H. Brune *C. R. Physique* **6** (2005) 75.
45. G. Autès, C. Barreteau, D. Spanjaard and M.-C. Desjonquères, *J. Phys. Condens. Matter* **18** (2006) 6785.
46. B. Schulz and K. Baberschke, *Phys. Rev. B* **50** (1994) 13467.
47. Z. Q. Niu, J. Pearson and S. D. Bader, *Phys. Rev. Lett.* **70** (1993) 1006.
48. R. Allenspach, M. Stampanoni and A. Bischof, *Phys. Rev. Lett.* **65** (1990) 3344.